Sedimentary Geology 494 (2026) 107029

Contents lists available at ScienceDirect

Sedimentary Geology

journal homepage: www.elsevier.com/locate/sedgeo

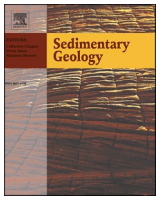

Influence of geomorphological dynamics and associated mineralogical structures on carbon mineralization processes within different surfaces of sand ramps

Mohsen Kargarian, Neda Mohseni *, Reza Hosseinzadeh

Department of Geography, Faculty of Letters and Humanities, Ferdowsi University of Mashhad, Mashhad, Iran

ARTICLE INFO

Editor: Dr. Massimo Moretti

Keywords:
XRD
XRF
Granulometry
Quaternary
Weathering
Erosion

ABSTRACT

Sand ramps are recognized as critical archives for reconstructing Late Quaternary environmental changes, including sediment supply, paleoclimate, and soil carbon dynamics. We investigated the influence of geomorphic processes, weathering, and mineralogical dynamics on the mechanisms controlling the sequestration and mineralization of soil organic carbon (SOC) within falling and climbing sand ramps. Analyses including XRD, XRF, SEM, granulometry, physicochemical attributes, and weathering indices were conducted on sand ramps in central Iran. The abundance of carbonate minerals, sand-sized sediments, well-sorted clastic aggregates, and symmetrical grain distribution, combined with high roundness and minimal quartz corrosion, suggests that falling surfaces remain relatively intact with limited evidence of weathering. Despite the presence of carbonate minerals on falling sand ramps, the lower proportion of clay minerals and fine particles resulted in weaker organic matter binding compared to climbing surfaces. Conversely, the higher frequency of secondary clay minerals, poor sediment sorting, high angularity, and the formation of micro-scale features on granites indicate long-term exposure of climbing surfaces to chemical weathering. The elevated presence of illite, kaolinite, montmorillonite, as well as Fe_2O_3 and Al_2O_3 oxides, supported pedogenic processes and promoted microaggregate-associated carbon, rendering SOC less accessible to microbial mineralization. The findings indicate that climbing sand ramps represent a stabilized, pedogenically altered colluvial-aeolian apron overlying the granite, where primary sedimentary structures have been obscured by chemical weathering and clay illuviation. This contrasts with the structurally intact, gravity-dominated falling ramps. These results suggest that localized variations in geomorphic and weathering processes, alongside mineralogical composition, significantly influence the biogeochemical mechanisms controlling SOC mineralization throughout the evolution of sand ramps, offering valuable insights into carbon dynamics in arid and semi-arid regions.

1. Introduction

Sand ramps are recognized as dune-scale sedimentary accumulations situated on a continuum of topographically controlled landforms, which includes alluvial fans and talus cones (Bateman et al., 2012; Rowell et al., 2018a). These features contain a complex assemblage of aeolian sands, paleosols, and interbedded fluvial deposits, making them key archives for recording Late Quaternary environmental changes, particularly regarding sediment supply, paleoclimate, and soil carbon dynamics (Kumar et al., 2017; Deng et al., 2023). The formation of discrete yet widespread climbing sand ramps on mountain slopes occurs in aeolian environments where locally sourced sands are mobilized by near-surface winds. When these migrating dunes encounter and ascend steep slopes (typically >10°), they form climbing (upwind) sand ramps (Chojnacki et al., 2010). Subsequently, these climbing ramps can act as sediment conduits, cascading over local topographical low points to become falling (downwind) ramps on the leeward slope.

The dynamics of geomorphic processes, influenced by varying environmental regimes, drive a continuum between aeolian topographic features and hillslope deposits within sand ramps. This results in significant heterogeneity regarding granulometry, mineralogy, morphoscopy, and physiochemical and biological attributes during the evolution of sand ramp structures (Rowell et al., 2018b; Hay et al., 2021). These localized variations control corridors for the sequestration

* Corresponding author.
E-mail address: nedamohseni@um.ac.ir (N. Mohseni).

https://doi.org/10.1016/j.sedgeo.2026.107029
Received 7 October 2025; Received in revised form 1 January 2026; Accepted 3 January 2026
Available online 8 January 2026

and mineralization of soil organic carbon within dryland landforms. The simultaneous operation of aeolian and hillslope processes on sand ramp surfaces facilitates sediment redistribution, preferentially removing carbon-enriched fine particles and entraining them into the atmosphere (Chappell and Baldock, 2016; Webb et al., 2017; Lal, 2019; Jiang et al., 2021). Neglecting these abiotic carbon fluxes, driven by wind and hillslope erosion, introduces significant uncertainty into ecosystem carbon accounting, especially in arid and semiarid environments highly susceptible to erosional processes.

Existing studies on sand ramps remain sparse, with the majority conducted in the Mojave Desert (Bateman et al., 2012), South Africa (Rowell et al., 2018a), and Namibia (Rowell et al., 2018b). These investigations indicate that sand ramp sediments consist largely of detrital minerals derived from parent material weathering, which are subsequently transported and deposited by physical agents such as wind and water. Additionally, del Valle et al. (2016) observed that sand ramps were often established under paleoclimate conditions and are currently relict features. Conversely, other research has demonstrated that some sand ramps remain active, with structures comprising a diversity of colluvium, alluvium, playa silts, and sand layers (Telfer et al., 2012; Jin et al., 2018; Kumar et al., 2017). Despite some research on the role of geomorphic processes in the formation and evolution of sand dunes in arid ecosystems (Chojnacki et al., 2010; Ellwein et al., 2015; Deng et al., 2023), detailed knowledge remains limited regarding how geomorphological dynamics stimulate localized variations in soil organic carbon dynamics throughout the evolution of sand ramp surfaces.

In this research, we aimed to elucidate how differences in the mineralogy, granulometry, and morphoscopic characteristics of falling and climbing sand ramps regulate the dynamics of biogeochemical processes controlling the sequestration and mineralization of soil organic carbon within these landforms. First, to explore the relationships between sand ramp evolution and their physical, biochemical, and mineralogical attributes, we examined localized variations in soil quality across different geomorphic surfaces of the ramps. Subsequently, to evaluate the biogeochemical processes governing soil organic carbon dynamics, we assessed the interplay between the evolution of ramp surfaces, geomorphological dynamics, and associated geochemical processes. The findings provide a foundation for developing restoration and geo-conservation strategies in arid and semi-arid regions characterized by high sensitivity to environmental disturbances.

2. Methods

2.1. Study sand ramps and sediment sampling

The sand ramps under investigation are situated in southern Yazd Province, Central Iran, located approximately at latitude 36° 30′ N and longitude 54° 00′ E (Fig. 1). This region is characterized by extensive sand ramp accumulations mantling the southwestern slopes of the Shirkouh granitoid massif. Geologically, the Shirkouh Massif constitutes a batholith extending over 1000 km^2. The lithology is dominated by granitic and granitoid units, overlain by a succession of Cretaceous limestone and dolomite exceeding 3000 m in thickness. Leucogranite outcrops within the Shirkouh complex are primarily composed of

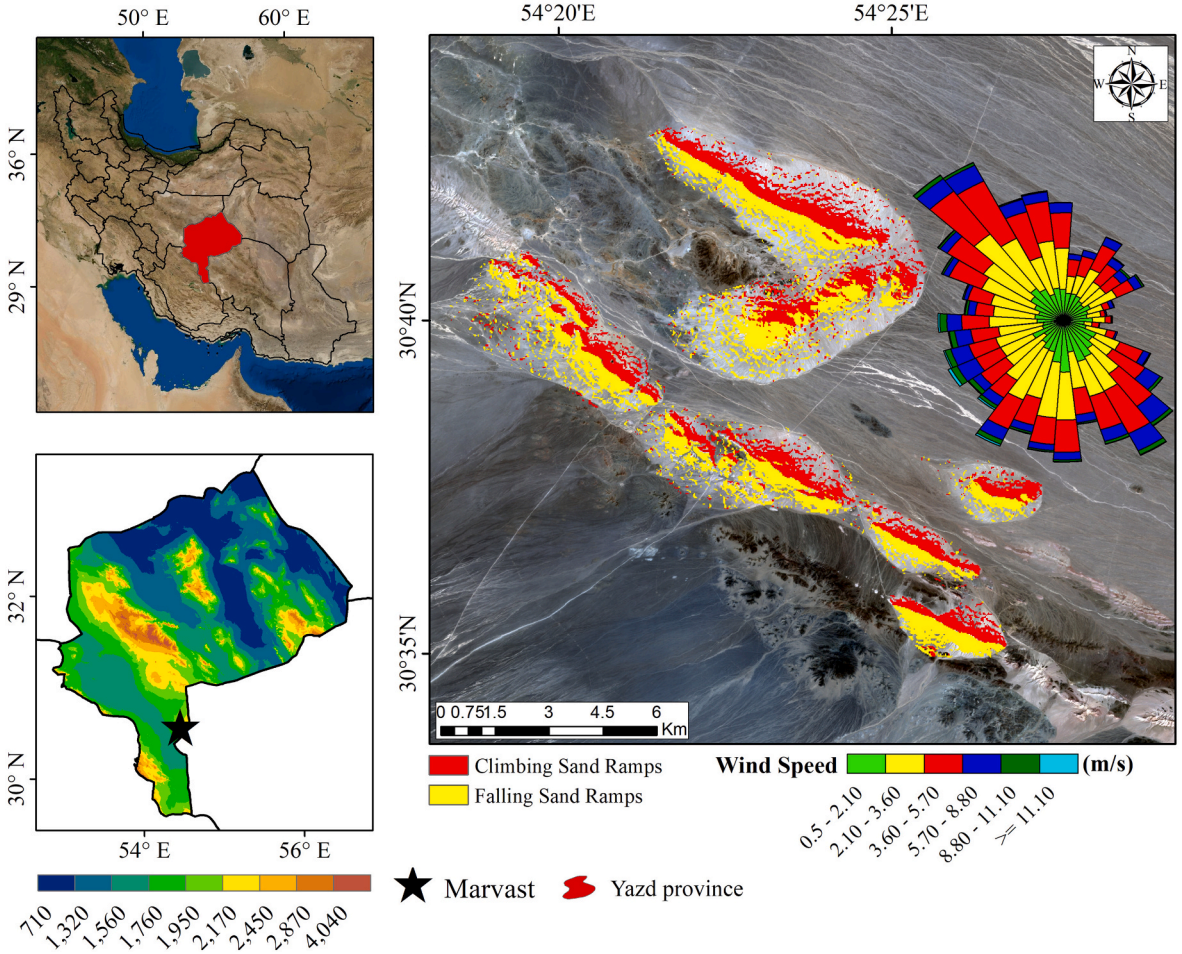

Fig. 1. Location of the study sand ramps in Central Iran. The position of falling and climbing sand ramps was determined by a windrose. Red area shows the windward position of climbing sand ramps along the direction of the prevailing wind, mainly northwest; Yellow area illustrates the leeward position of falling sand ramps, along the southeasterly and southwesterly winds.

quartz, feldspar (including sodic plagioclase and K-feldspar), and biotite. The petrological assemblage of the batholith comprises plagioclase, quartz, feldspars, muscovite, tourmaline, cordierite, biotite, monazite, and zircon-apatite (Sheibi and Esmaelly, 2009). The Shirkouh batholith incorporates magmatic segments of Jurassic origin, succeeded by the discontinuous deposition of Cretaceous conglomerates and carbonates. The Laramide orogeny induced the folding of these sedimentary sequences, ultimately resulting in the structural uplift of the Shirkouh massif. Surrounding the study area, carbonate facies (limestone and dolomite) predominate, whereas granitic exposures are restricted to higher elevations, valleys, and glacial cirques, having been exhumed by Quaternary glacial erosion.

Two active, sub-parallel dextral strike-slip faults—the Dehshir Fault to the east and the Anar Fault to the west—have played a pivotal role in the morphogenesis of the sand ramps, alluvial fans, and ephemeral drainage systems. The Marvast Playa, which hosts the studied sand ramps, is situated within a zone dynamically controlled by both the Dehshir and Anar fault systems. Consequently, the Marvast Playa represents a complex geomorphic product resulting from the interplay of tectonic processes confined between these two major fault systems and variable climate conditions throughout the Quaternary.

These faults have generated shallow accommodation space, creating ideal environments for sediment accumulation. The active neotectonics associated with these two NW–SE trending fault systems have generated subsiding basins that act as depocenters for evaporites and aeolian sediments, which are typical of the study region. The Dehshir Fault, extending approximately 400 km, is a structural feature of significant long-term tectonic activity, governing major displacements within the Central Iranian Range since the Eocene–Oligocene. Its southern segment directly influences surface environments, dissecting Quaternary lacustrine deposits, wetlands, and playas. Occurrences of travertine along the fault trace provide evidence of a paleo-humid climate, contrasting with current arid conditions, thereby highlighting the interplay between climate fluctuations and tectonic activity over varying temporal scales.

The Anar Fault, with a length of approximately 345 km, constitutes a major structural element; its northern segment exhibits clear displacement of Quaternary sediments and offsets geological structures along its strike. The regional geomorphology is defined by three dominant units: (1) Alluvial fans, composed of coarse-grained sediments and Holocene alluvium accumulated on the piedmonts; (2) Playa surfaces (e.g., Marvast), representing the floors of intermediate plains where the prevailing arid climate fosters seasonal evaporation, mudflat development, and salt marsh formation; and (3) Sand ramps.

Based on meteorological data acquired over a distinct 25-year period (1996–2020), the study area exhibits a mean annual temperature of 18.02 °C (Fig. 2). The thermal regime is characterized by distinct seasonality, where July represents the thermal maximum with a mean maximum temperature of 38.71 °C and a monthly mean of 29.78 °C.

Fig. 2. Meteorological data acquired by the Marvast synoptic station over a 25-year period (1995–2020).

Conversely, January records a mean minimum temperature of −1.04 °C, confirming the prevalence of nocturnal freeze-thaw cycles during the winter season. The pronounced differential between the mean minimum of the coldest month and the mean maximum of the warmest month indicates an annual thermal amplitude of approximately 40 °C. This high amplitude reflects the low specific heat capacity of the surficial environment, attributable to the scarcity of vegetation cover and soil moisture deficit. During the Last Glacial Period of the Quaternary, the region experienced a colder and moister climate, with temperatures approximately 9 °C lower than present conditions (Fig. 3).

Precipitation analysis classifies the Marvast region within the hyper-arid to arid climate spectrum, with a mean annual precipitation of 65.91 mm (Fig. 2). The temporal distribution of precipitation is uneven, with winter being the dominant wet season, receiving 30.53 mm (approximately 46% of the total annual input). These precipitation events are primarily driven by the incursion of Mediterranean and Sudanese low-pressure systems.

Regarding the aeolian regime, the mean annual wind velocity is calculated at 3.26 m/s, suggesting relatively quiescent conditions on a general scale (Fig. 2). However, wind activity exhibits significant seasonal variability. Spring represents the most turbulent season, with mean maximum velocities reaching 8.05 m/s. Specifically, April records the highest wind speeds (8.24 m/s), a phenomenon likely resulting from intensified pressure gradients and atmospheric instabilities characteristic of the seasonal transition. The resultant mean annual wind vector is 290.85°, indicating a prevailing wind direction from the West-Northwest. Furthermore, the identification of two distinct wind directional patterns—Western/Southwestern flows in winter versus Northern/Northeastern flows in summer—suggests that the region is modulated by differing macro-scale synoptic circulation patterns throughout the annual cycle.

To distinguish between the distinct surfaces of sand ramps, we established classification criteria based on the interaction between airflow, topography, and sediment supply, following frameworks suggested by Bateman et al. (2012), Telfer et al. (2012), and Rowell et al. (2018a, 2018b). (1) As a primary criterion, we utilized the prevailing wind direction derived from a 30-year windrose at the Marvast synoptic station (Fig. 1). Climbing sand ramps typically develop on windward slopes aligned with the prevailing northwest wind, whereas falling sand ramps are predominantly oriented towards the southeast and southwest (Fig. 1). Consequently, landforms situated on the leeward side—within zones of flow separation or expansion downstream of the crest line—were identified as potential falling ramps (Fig. 4A & C). Conversely, features located on the windward side of topographic obstacles, characterized by zones of airflow compression, were preliminarily classified as climbing ramps (Fig. 4B & D). (2) Field observations regarding morphological characteristics indicate that climbing ramps, which are influenced significantly by hillslope and runoff processes, exhibit a wedge-shaped morphology that thins upslope. These forms typically initiate at the base of steep slopes (>10°) before ascending. This configuration facilitates the accumulation of a substantial layer of alluvial deposits (Fig. 4B & D). These features demonstrate a topography-opposing transport vector. Furthermore, the admixture of fluvial sediments and weathered materials on these ramps promotes denser vegetation cover compared to falling surfaces. In contrast, falling ramps appear as cascading lobes or tongues exhibiting gravity-assisted transport; they often maintain steep gradients approaching the angle of repose near the crest, flattening distally. Field identification of climbing ramps further relied on their onlapping relationship with bedrock and interbedding with colluvial material derived from upper slopes, often displaying massive or crude stratification resulting from the interplay of saltation and slope-wash processes. (3) Following the differentiation of

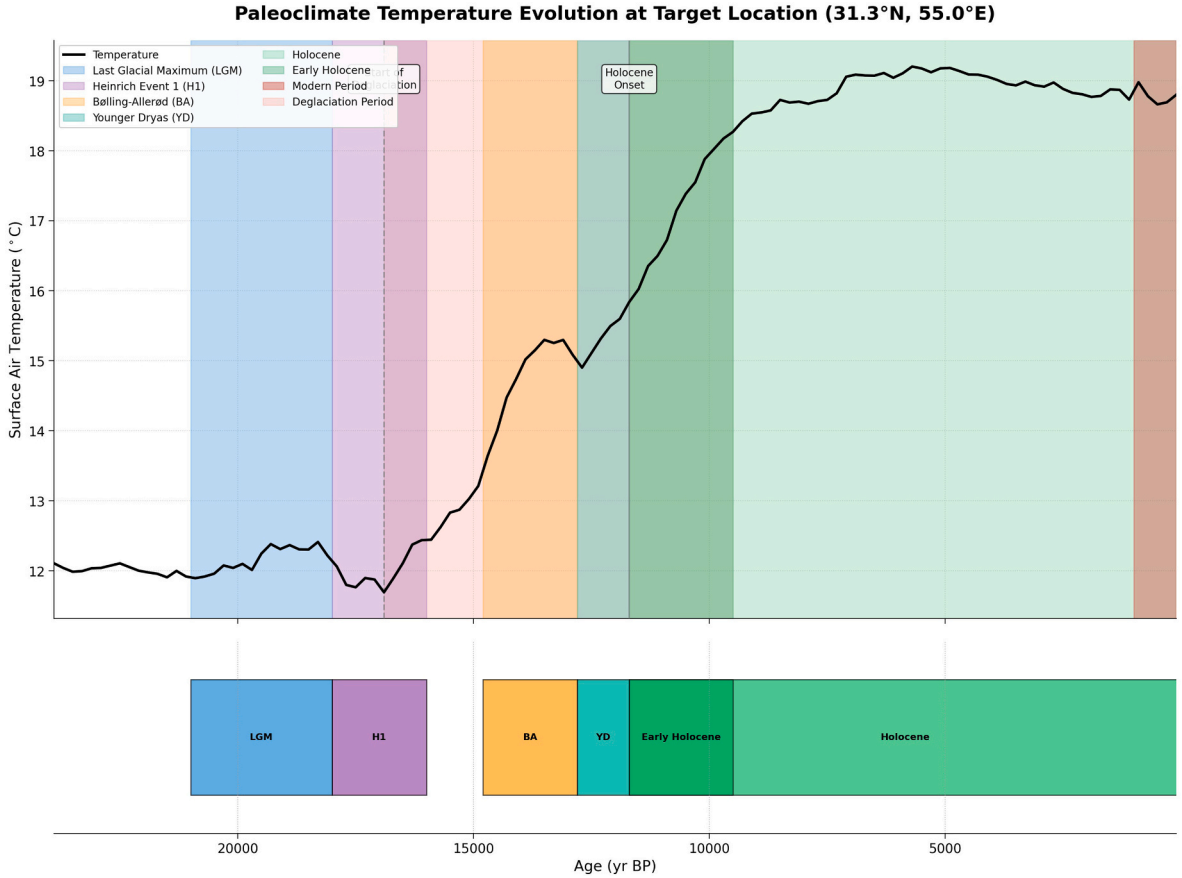

Fig. 3. Reconstruction of the late Quaternary period.

Fig. 4. Field observations of falling (A-C) and climbing (B—D) sand ramps covered by a substantial layer of alluvial deposits and vegetation.

windward and leeward slopes, the precise coordinates of each sand ramp were recorded during field surveys using a handheld GPS (Garmin eTrex 32×; ~ ± 3 m accuracy).

Given the aeolian origin and highly dynamic nature of sand ramps in Central Iran's arid environment, pedogenesis is generally limited, and soil horizon development is poorly expressed. Field surveys revealed no laterally continuous or well-developed diagnostic soil horizons, particularly on falling sand ramps. Consequently, observations focused on surface and near-surface morphological indicators, such as sediment cohesion, surface crust development, and colour variations in the upper soil layers. These features, integrated with Scanning Electron Microscopy (SEM) observations and laboratory-based mineralogical and geochemical analyses, were utilized to infer early-stage pedogenic processes and mechanisms of soil organic matter stabilization.

In total, 50 sediment samples were collected from climbing ramps and 50 from falling ramps at a depth of 0–30 cm. For the assessment of biological properties and bacterial/fungal enumeration, sediment subsamples were transported to the laboratory on dry ice. Large organic debris and stones were subsequently removed, and following sieving through a 2 mm mesh, samples were stored at 4 °C. To determine soil bulk density, intact sediment cores were obtained using cylinders measuring 30 cm in depth and diameter.

2.2. Granulometry and stability indices analysis

Particle size distribution, geometric mean diameter (GMD), and mean weight diameter (MWD) were determined using the wet-sieving technique (Kemper and Rosenau, 1986). Calculations for GMD and MWD were performed according to Mazurak (1950) and Bavel (1949), respectively. Sediment transport dynamics were inferred from granulometric parameters derived from Folk and Ward (1957). Specifically, the mean grain size provided an estimate of the average particle diameter within the sediment. Skewness characterized the asymmetry of the grain size distribution; positive values denote finer sediments, negative values suggest coarser material, and a value of zero implies symmetry. Sorting was calculated to illustrate particle size variability and the magnitude of deviation from the mean, while kurtosis assessed the degree of peakedness or sorting in the distribution tails.

$$\text{Mean grain size (Mz)} = \frac{\varnothing 16 + \varnothing 50 + \varnothing 84}{3}$$

$$\text{Skewness } (SKI) = \frac{\varnothing 16 + \varnothing 84 + 2\varnothing 50}{2\,(\varnothing 84 - \varnothing 16)} + \frac{\varnothing 5 + \varnothing 95 + \varnothing 50}{2\,(\varnothing 95 - \varnothing 5)}$$

$$\text{Kurtosis}(KG) = \frac{\varnothing 95 + \varnothing 5}{2.44\,(\varnothing 75 - \varnothing 25)}$$

$$\text{Sorting } (\sigma) = \frac{\varnothing 84 + \varnothing 16}{4} + \frac{\varnothing 95 + \varnothing 5}{6.6}$$

2.3. Sediment biochemical analysis

Sediment bulk density (BD, cm^{-3}) was measured following the core method described by Blake and Hartge (1986), calculated as the ratio of oven-dried sediment mass to core volume. Total porosity (TP, %) was subsequently derived from the values of sediment bulk density and particle density (Beylich et al., 2010). Calcium carbonate equivalent (CCE, %) was quantified utilizing the acid neutralization method (Loeppert and Suarez, 1996). Electrical conductivity (EC) of the saturated paste extract and sediment pH were determined using standard electrometric methods (Richards, 1954). Soil organic carbon (SOC, kg^{-1}) was quantified using the Walkley–Black wet oxidation technique (Rowell, 1994). To ensure the exclusive measurement of organic carbon, samples underwent pretreatment with dilute HCl to eliminate inorganic carbonates, followed by thorough washing with deionized water and drying at $40^{\circ}C$.

Carbon mineralization dynamics were assessed by quantifying soil microbial respiration (RS), the C mineralization ratio, and microbial activity. RS ($mg\ CO_2\ kg^{-1}\ soil\ day^{-1}$) was measured via the alkali-trapping method described by Rabbi et al. (2014). The carbon

mineralization ratio was subsequently calculated as the quotient of evolved $CO_2$to total SOC. Microbial activity was evaluated through bacterial and fungal enumeration (Wollum, 1982). A suspension was prepared by dispersing 10 *g*of sediment in 90 *mL*of sterile water. For bacterial counts, 0.1 *mL*aliquots from serial dilutions were inoculated onto Nutrient Agar plates in triplicate and incubated at 28°*C*for one week. Similarly, fungal populations were enumerated by plating 0.1 *mL*from serial dilutions onto Martin Agar supplemented with rose bengal and streptomycin, followed by incubation at 28–30°*C*for one week.

Sediment organic carbon fractionation was performed using physical fractionation techniques (Six et al., 2002). Total SOC was separated into three discrete fractions following Doetterl et al. (2016): SOC > 250 μm, representing unprotected particulate organic carbon; SOC 53–250 μm, corresponding to carbon occluded within microaggregates; and SOC < 53 μm, representing mineral-associated organic carbon linked to clay and silt.

2.4. Chemical weathering index

To quantify the influence of parent material weathering on soil carbon fractions, chemical weathering indices were calculated, specifically the Ruxton Ratio (R), the Chemical Index of Weathering (CIW), and the Chemical Index of Alteration (CIA). The Ruxton Ratio (Ruxton, 1968) incorporates the SiO_2/Al_2O_3 and SiO_2/Fe_2O_3 ratios. The CIA, formulated by Nesbitt and Young (1982), was employed to assess the transformation of primary minerals into secondary phases. This index utilizes the molar proportions of Al_2O_3, CaO, MgO, Na_2O, and K_2O. The CIW, introduced by Harnois (1988), accounts for the same major oxides as the CIA, with the exclusion of K_2O.

$$R = \frac{SiO2}{Al2O3} \quad Fresh\ material > 10$$

$$R = \frac{SiO2}{Fe2O3} \quad Fresh\ material < 10$$

$$CIA = \frac{Al2O3}{Al2O3 + CaO + Na2O + K2O} \times 100 \quad Fresh\ material \leq 50$$

$$CIW = \frac{Al2O3}{Al2O3 + CaO + Na2O} \times 100 \quad Fresh\ material \leq 50$$

2.5. XRD, XRF, and SEM analysis

To determine the mineralogical composition of the sand ramp surfaces, X-ray diffractometry (XRD) and X-ray fluorescence (XRF) spectrometry were utilized. Mineralogical composition was assessed via semi-quantitative XRD analysis based on peak intensity ratios. Each mineral phase was quantified independently relative to its reference pattern, rather than through full-pattern Rietveld refinement. Consequently, the reported values represent relative abundance indices rather than absolute weight percentages, and their sum is not constrained to 100%.

The total concentrations of oxides, including SiO_2, CaO, Na_2O, K_2O, Al_2O_3, and Fe_2O_3, were determined using an X-ray fluorescence spectrometer. Additionally, the determination of major elements was conducted using Inductively Coupled Plasma-Atomic Emission Spectroscopy (ICP-AES), while Loss on Ignition (LOI) was measured via gravimetric analysis. The detection limit for the major elements ranged between 0.01 and 0.1 wt%.

To investigate particle morphology and surface micro-textures, scanning electron microscopy (SEM) was performed on selected grain-size fractions. Sediment samples were initially air-dried at room temperature and gently disaggregated using a rubber pestle to prevent artificial grain breakage. Subsequently, the samples were dry-sieved to isolate the sand-sized fraction (63–500 μm) for SEM analysis. This analysis was intentionally restricted to the coarse fraction, excluding the finer silt and clay fractions, which were instead characterized indirectly via XRD. The sand fraction was selected as it is widely regarded as the most representative size range for identifying transport-related micromorphological features and distinguishing between aeolian and fluvial processes. Representative quartz and feldspar grains were hand-picked under a binocular microscope, mounted on aluminum stubs using conductive carbon tape, and coated with a thin gold/palladium layer to ensure electrical conductivity. Grain morphology, roundness, surface textures, and weathering characteristics were examined and qualitatively compared to infer variations in sediment transport history and provenance.

For the quantitative assessment of grain morphology, SEM images were utilized to analyze 870 individual grains using ImageJ-based algorithms (Python/OpenCV) (Pinet et al., 2019). Projected area, perimeter, and shape descriptors (specifically circularity, solidity, and elongation/aspect ratio) are widely recognized indicators for determining transport conditions (Joo et al., 2018; Van Hateren et al., 2020; Varga et al., 2021; Martewicz et al., 2022). The circularity coefficient (C), which ranges from 0 to 1, represents the ratio between the projected area (S, μm^2) and the squared perimeter (P) of each particle, calculated as $C = 4\pi \times S / P^2$ (Pinet et al., 2019). The equivalent diameter (Deq) of each particle was derived using the formula $(S/\pi)^{1/2}$.

The aspect ratio is defined by the ratio of the width to the length of the analyzed grain, expressed as 1 - (Width / Length). Generally, an aspect ratio deviating from 1 indicates elongated particles, whereas a value equal to 1 represents a perfect circle (Gresina et al., 2023). Grain solidity, which indicates the degree of protrusion or depression, is calculated as the ratio of the particle's area to the area enclosed by its convex hull (Gresina et al., 2023).

2.6. Evaluation of soil quality index

To identify key indicators controlling soil quality across different sand ramp surfaces, a Minimum Data Set (MDS) was established using Principal Component Analysis (PCA) (Andrews et al., 2002). The PCA was performed on 26 physical and biochemical sediment properties, along with four weathering indices (Table 1). Principal Components (PCs) with eigenvalues greater than or equal to 1 were retained for the MDS selection (Li et al., 2024). Within each PC, only variables with loading values within 10% of the highest weighted loading were considered candidates for indexing. Based on Pearson's correlation analysis, if no significant correlation existed between highly loaded variables, each was included in the MDS. Subsequently, non-linear scoring functions were employed to convert MDS variables into unitless scores ranging from 0 to 1 (Tesfahunegn, 2014; Damiba et al., 2024). Finally, weighting factors were assigned to calculate the Soil Quality Index (SQI) following the equation outlined by Armenise et al. (2013):

$$SQI = \sum_{i=1}^{n} W_i S_i$$

where S_i shows a non-linear score; W_i explains the PCA-derived weighting factor.

2.7. Reconstruction of the paleoclimate

To examine paleoclimate variations in the study region, the “Globally Resolved Surface Temperatures Since the Last Glacial Maximum” dataset (Osman et al., 2021) was utilized. This dataset provides a proxy-constrained reconstruction of global surface temperatures over the past 24,000 years at 200-year intervals. Data were sourced from the NOAA Paleoclimatology Database (https://www.ncei.noaa.gov/access/paleo-search/study/33112). Processing was conducted using Python scripts within the Google Colab environment. Modules such as Pandas, Matplotlib, and SciPy were incorporated for data manipulation,

Table 1
Bio-physiochemical characteristics, major elements, base cations, and weathering indices of the studied sand ramps.

Sediment Variables	Climbing sand ramp	Falling sand ramp
SOC g kg^{-1}	$43.85^{a} \pm 1.12$	$31.06^{b} \pm 2.45$
SOC, < 53 μm (g kg^{-1})	$12.91^{a} \pm 2.16$	$7.51^{b} \pm 2.39$
SOC, 53-250 μm (g kg^{-1})	$20.57^{a} \pm 1.11$	$8.86^{b} \pm 2.21$
SOC, > 250 (g kg^{-1})	$9.54b^{b} \pm 1.06$	$14.29^{a} \pm 2.45$
MWD (mm)	$0.59^{a} \pm 0.14$	$0.48^{b} \pm 0.18$
GMD(mm)	$0.52^{a} \pm 0.09$	$0.45^{b} \pm 0.23$
BD (gr cm^3)	$1.21^{b} \pm 0.04$	$1.71^{a} \pm 0.04$
PD (gr cm^3)	$2.14^{b} \pm 0.26$	$2.75^{a} \pm 0.15$
TP (%)	$39.81^{a} \pm 1.89$	$28.49^{b} \pm 1.35$
VWC (%)	$18.85^{a} \pm 1.33$	$16.65^{b} \pm 1.18$
EC (%)	$5.94^{b} \pm 6.59$	$6.32^{a} \pm 6.96$
CCE (%)	$36.68^{b} \pm 1.43$	$57.94^{a} \pm 1.87$
pH	$8.01^{b} \pm 0.69$	$8.74^{a} \pm 0.53$
RS mg CO_2/kg soil day	$6.25^{b} \pm 0.93$	$8.16^{a} \pm 0.84$
C mineralization (%)	$8.26^{b} \pm 1.83$	$18.35^{a} \pm 2.11$
Bacterial (CFU/g)	$67.5^{b} \pm 2.20$	$75.5^{a} \pm 2.50$
Fungal (CFU/g)	$4750^{b} \pm 8.82$	$6000^{a} \pm 6.67$
CIW (%)	$79.81^{a} \pm 3.21$	$56.67^{b} \pm 1.19$
R (SiO_2/Al_2O_3)	$2.81^{b} \pm 0.43$	$5.16^{a} \pm 0.65$
R (SiO_2/Fe_2O_3)	$6.11^{b} \pm 0.54$	$10.73^{a} \pm 0.78$
CIA (%)	$73.93^{a} \pm 4.43$	$48.8^{b} \pm 3.43$
Fe_2O_3 (%)	$7.52^{a} \pm 0.36$	$5.03^{b} \pm 0.42$
Al_2O_3 (%)	$16.37^{a} \pm 1.65$	$10.45^{b} \pm 1.76$
K_2O (%)	$1.63^{b} \pm 0.32$	$2.97^{a} \pm 0.25$
Na_2O (%)	$1.02^{b} \pm 0.08$	$2.23^{a} \pm 0.23$
CaO (%)	$3.12^{b} \pm 0.93$	$5.76^{a} \pm 0.87$
SiO_2 (%)	$46.40^{b} \pm 1.76$	$54.27^{a} \pm 2.43$

The values presented are based on mean ± standard error of the means, $n = 100$. 50 falling sand ramps and 50 climbing sand ramps. Lowercase letters indicate statistically significant differences ($P < 0.05$) between the sand ramp surfaces. CaO represents the CaO incorporated in the silicate fraction and corrected for carbonate minerals (Nesbitt and Young, 1982). All the element oxides are expressed by molar fraction.

visualization, and statistical assessment of temperature anomalies, respectively, enabling a robust quantification of long-term climate trends and their implications for the region.

2.8. Data analysis

Initially, the dataset was evaluated for normality using the Kolmogorov-Smirnov test. Subsequently, an independent samples *t*-test ($P < 0.05$) was conducted to determine significant differences in mineralogical, physicochemical, and biological properties between falling and climbing sand ramps. Correlation analysis was performed to identify the controlling factors influencing Soil Organic Carbon (SOC) sequestration across different sand ramp surfaces. Finally, stepwise multiple regression was employed to evaluate the relationships between sand ramp evolution and the biochemical processes regulating C mineralization. All statistical analyses were executed using the Python programming language.

3. Results

3.1. Biochemical properties of different surfaces of sand ramps

As presented in Table 1, total SOC and associated biochemical properties exhibited statistically significant variations between falling and climbing sand ramps. Total SOC was significantly higher in climbing sand ramps (43.85 $g\,kg^{-1}$) compared to falling surfaces (31.06 $g\,kg^{-1}$). For climbing surfaces, the majority of carbon was concentrated within the 53–250 μ*m* fraction, accounting for 46.9%of total SOC. The finer (< 53 μ*m*) and coarser (> 250 μ*m*) fractions contributed 29.44%and 21.75%to total SOC, respectively. Generally, climbing surfaces exhibited higher carbon content associated with microaggregates (53–250 μ*m*) and clay-silt aggregates (< 53 μ*m*) relative to falling sand ramps. Conversely, unprotected SOC (> 250 μ*m*) content was notably higher (46%) in falling surfaces compared to climbing sand ramps. In falling sand ramps, the < 53 μ*m* and 53–250 μ*m* fractions accounted for 24.17%and 28.2%of total SOC, respectively. Within climbing sand ramps, clay and silt content, aggregate stability indices, moisture, and total porosity were significantly elevated, whereas pH, bulk density (BD), electrical conductivity (EC), and calcium carbonate equivalent (CCE) values were lower. Regarding microbial quantification, falling sand ramps exhibited higher bacterial (75.5 $CFU\,g^{-1}$) and fungal (6000 $CFU\,g^{-1}$) populations compared to climbing surfaces. Furthermore, the C mineralization ratio and microbial respiration showed a statistically significant increase within falling sand ramps compared to climbing surfaces.

3.2. Elemental (XRF), mineralogical (XRD), SEM, and granulometry analyses

Based on the XRF results (Table 1), base cation contents—including SiO_2, CaO, Na_2O, and K_2O—were significantly higher in falling sand ramps. Conversely, contents of Al_2O_3 and Fe_2O_3 showed a statistically significant increase in climbing sand ramps. Sediments on climbing surfaces appeared more extensively weathered, indicated by reduced R values and elevated CIW and CIA values compared to those on falling surfaces (Table 1). As shown in Table 1, the CIA values of the climbing sand ramps range between 70 and 80, reflecting a moderately weathered state. In contrast, the CIA values of the falling surfaces range between 50 and 60, indicating a very slightly weathered state (Nesbitt and Young, 1982).

According to the XRD results, the dominant minerals in climbing surfaces were orthoclase, dolomite, calcite, halite, and albite (Table 2). The dominant mineral in falling sand ramps was quartz (> 50%). Calcite (38.90%), albite (30.70%), orthoclase (26.20%), dolomite (27.65%), and halite (25.00%) were also detected on these surfaces (Fig. 5a-c). Secondary clay minerals, including illite (38.74%), kaolinite (36.60%), and montmorillonite (37.20%), constituted the largest mineral fraction of the climbing sand ramps (Fig. 5d-f).

To better understand the evolution of these landforms, climbing and falling surfaces were granulometrically analyzed (Table 3). The granulometry results showed that falling sand ramps are dominated mainly by sand-sized sediments (49.34%). Higher concentrations of clay (39.97%) and silt (31.81%) sediments were observed in climbing surfaces compared to falling surfaces. As shown in Table 3, the sediment distribution in climbing sand ramps was highly asymmetrical and exhibited poorer sorting compared to falling sand ramps. Skewness values ranged between − 0.004 and + 0.23. Sediments of climbing sand ramps are fine-skewed (positive), whereas falling surfaces are coarse-skewed to near-symmetrical (negative) (Table 3). Mean grain size ranged from 1.42ϕ(medium-grained) in falling sand ramps to 3.27ϕ(fine-grained) in climbing surfaces. Kurtosis values illustrated a range from 0.74 (very platykurtic) in climbing sand ramps to 1.35 (leptokurtic) in falling surfaces.

Table 2
Frequency of the identified minerals from XRD analysis.

XRD Pattern (%)/ sand ramp surface	Falling	Climbing
Calcite	49.90	22.80
Quartz	51.70	7.03
Albite	30.70	–
Orthoclase	35.20	1.80
Illite	–	38.74
Kaolinite	–	35.60
Montmorillonte	8.10	37.20
Dolomite	27.65	16.70
Gypsum	19.17	3.10
Halite	25.00	1.80

Note: Halite refers to crystalline sodium chloride (NaCl).

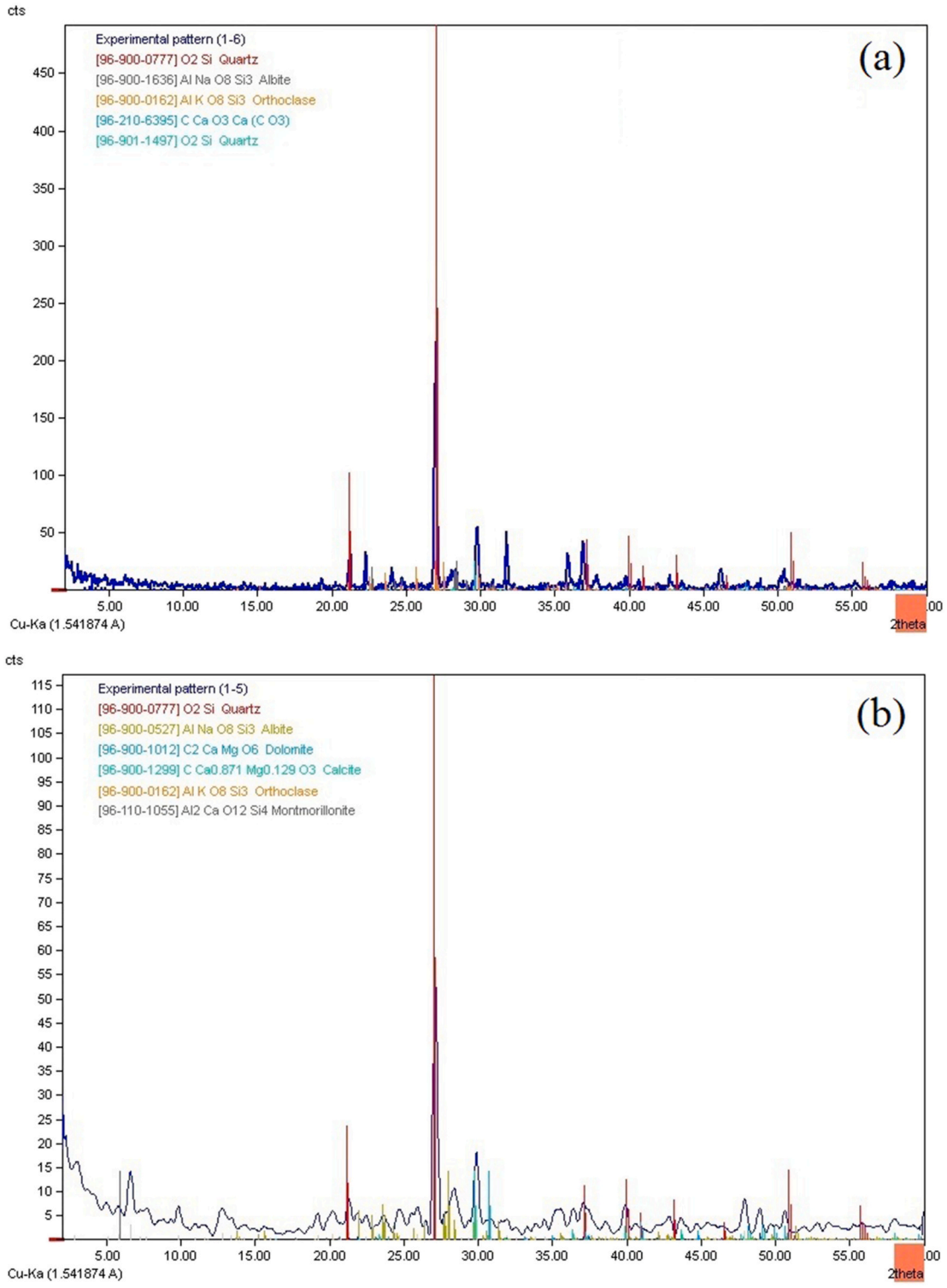

Fig. 5. X-ray diffractogram of falling (panel a-c) and climbing (panel d-f) sand ramps.

Sediment grain roundness, weathering, and corrosion were evaluated using morphoscopic analysis (Fig. 6). The falling sand ramp sediments were rounded and non-angular, lacking shelter fractures resulting from mechanical friction. However, the climbing surface sediments were not rounded (angular), reflecting notable evidence of erosion and corrosion. Statistical analysis of grain morphology reveals a significant difference ($p < 0.001$) in mean circularity, mean solidity, and mean elongation between climbing and falling grains (Table 3). Climbing grains are characterized by lower circularity (0.48), roundness (0.35), solidity (0.45), and higher elongation values (1.72) compared to falling grains. In contrast, falling grains exhibited significantly higher mean circularity (0.87), roundness (0.78), and solidity (0.52) and lower mean elongation (1.05), reflecting smoother edges and higher roundness.

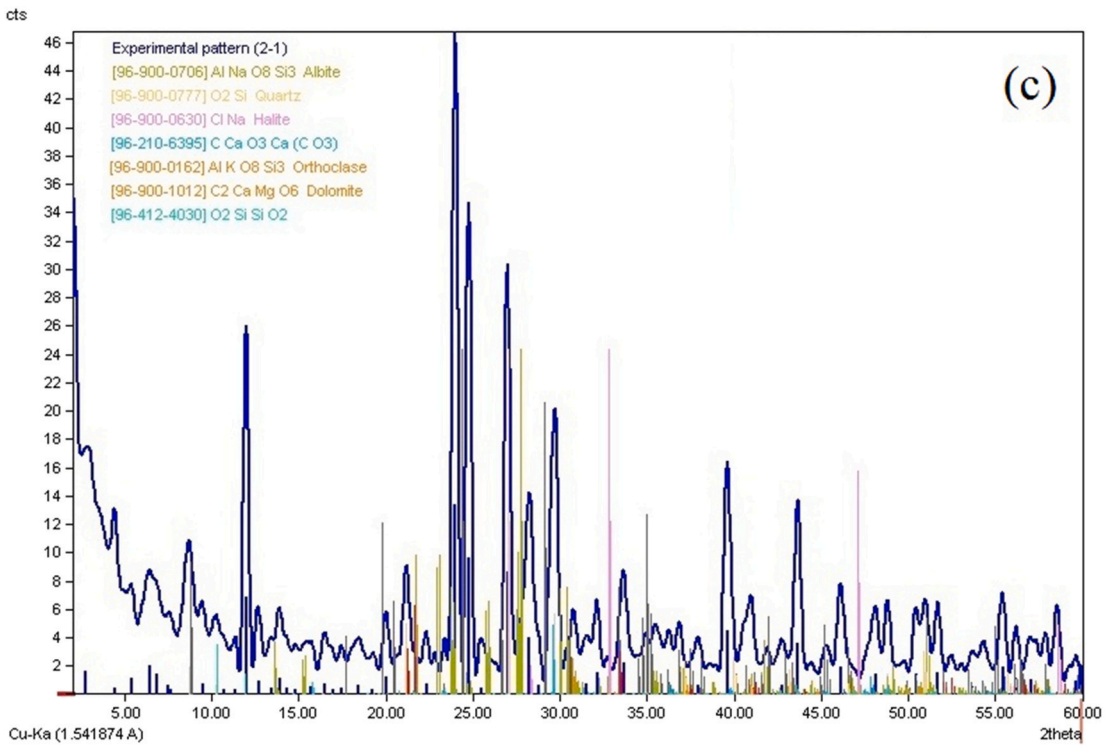

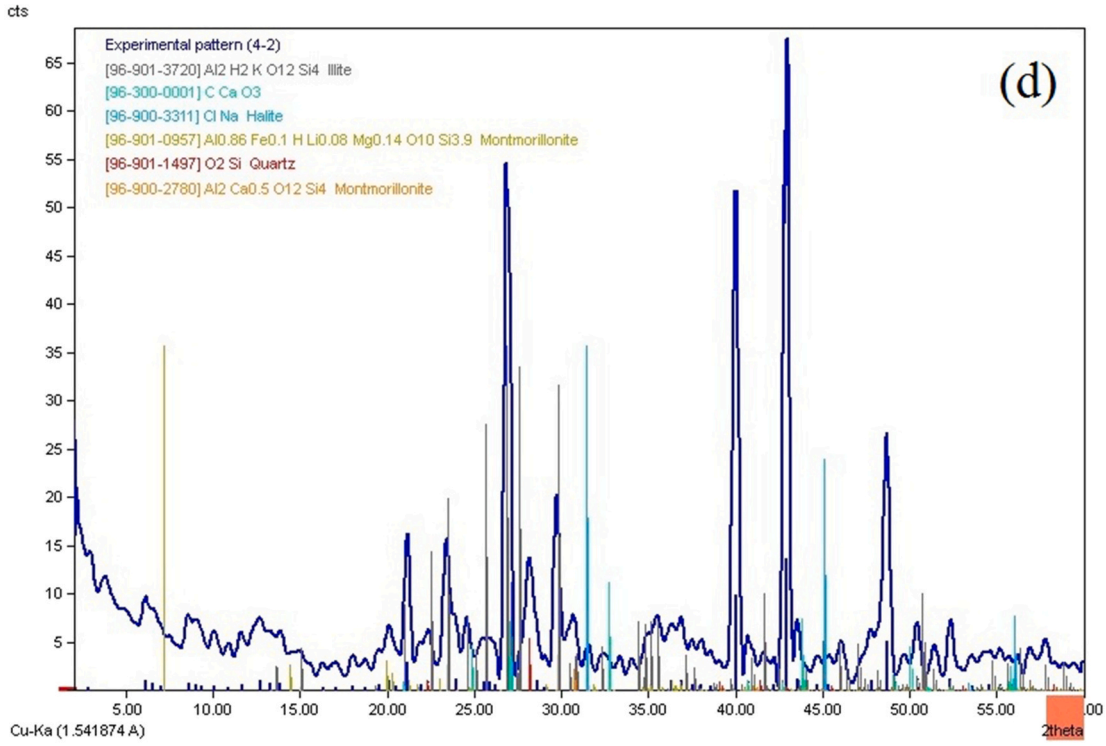

Fig. 5. (*continued*).

3.3. Carbon mineralization and geochemistry of falling and climbing sand ramps

The Pearson correlation analysis revealed that total SOC within falling sand ramps was significantly correlated with the >250 μm SOC fraction (positively), CCE (negatively), and pH (negatively) (Table 4). On climbing surfaces, the SOC 53–250 μm fraction, MWD, CIA, GMD, R, Fe_2O_3, and bacterial populations were significantly positively correlated with total SOC. Stepwise multiple linear regressions demonstrated the relationship patterns between C mineralization and the geochemistry of the sand ramps (Table 5). For falling sand ramps, the independent variables identified as controlling C mineralization were the bacterial

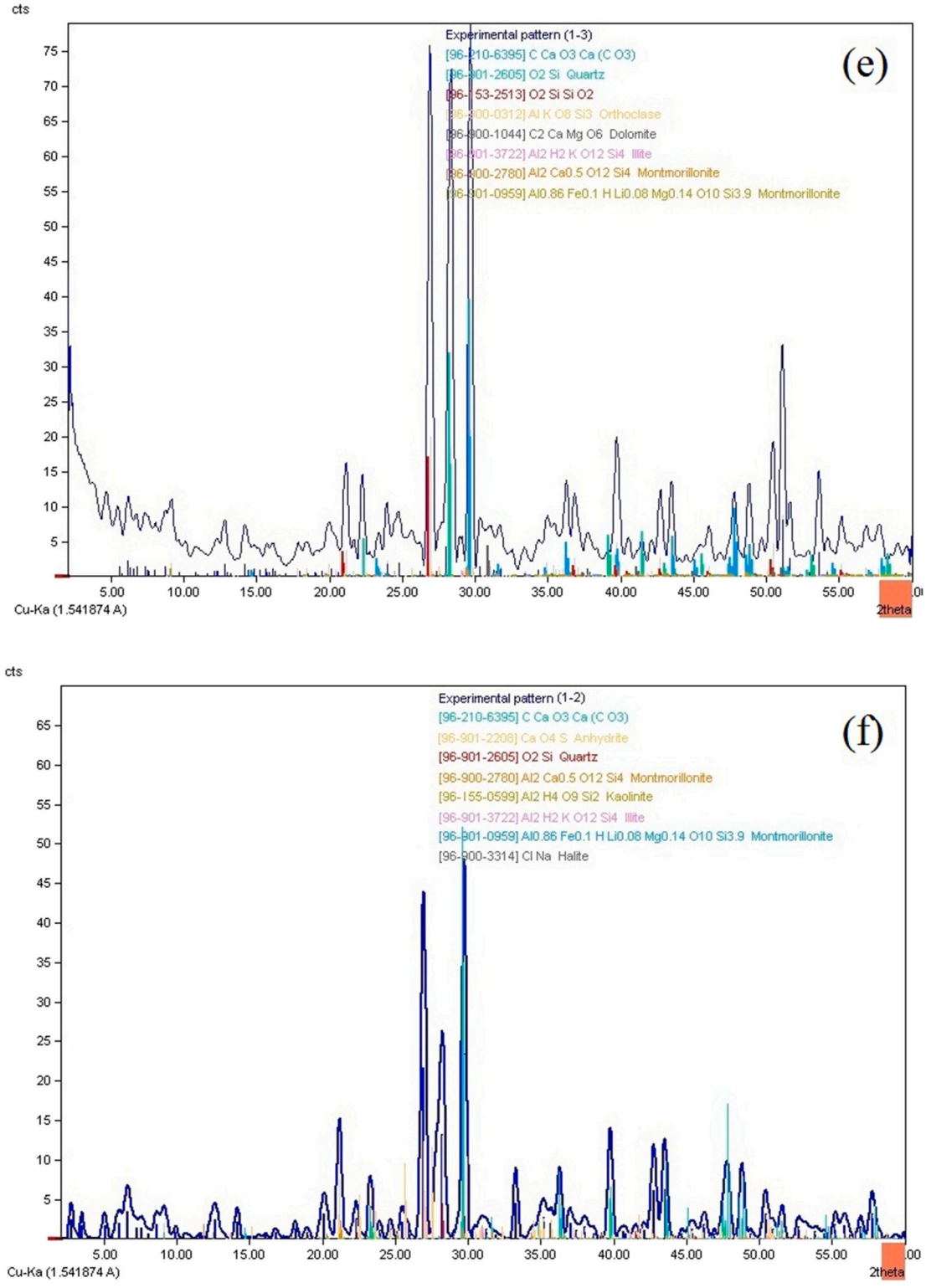

Fig. 5. (*continued*).

population and unprotected SOC (>250 μm). These factors exerted a significant positive impact on the C mineralization ratio. Conversely, on climbing surfaces, MWD, Fe_2O_3, GMD, the SOC 53–250 μm fraction, and CIW were found to have a significant negative impact on the carbon mineralization ratio.

3.4. Contribution of PCA-chosen MDS to the soil quality index within sand ramps

The Principal Component Analysis (PCA) results revealed significant differences in the physicochemical attributes between the studied sand ramps (Fig. 7). The first principal component (PC1) exhibited an eigenvalue greater than 1, accounting for a substantial 69.08% of the total variability. Within PC1, several attributes displayed high

Table 3
Statistical results of the SEM and granulometry analysis.

Statistical parameters	Climbing grains	Falling grains
Mean Circularity	0.48 ± 0.14	0.87 ± 0.08
Mean Solidity	0.45 ± 0.11	0.91 ± 0.05
Mean Aspect Ratio	1.86 ± 0.35(Elongated)	1.05 ± 0.18 (Equant)
Mean Roundness	0.35 ± 0.12	0.78 ± 0.10
Clay (%)	39.97^{a} ± 2.34	28.12^{b} ± 2.86
Silt (%)	31.81^{a} ± 2.98	21.79^{b} ± 1.54
Sand (%)	27.34^{b} ± 3.11	49.34^{a} ± 4.32
Sorting	0.75^{b} ± 0.13	2.46^{a} ± 0.09
Skewness	0.23 ± 0.06	−0.004 ± 0.01
Kurtosis	0.74^{b} ± 0.02	1.35^{a} ± 0.04
Mean grain size	3.27 ϕ	1.42ϕ

The values presented are based on mean ± standard deviation of the means. All values indicate statistically significant differences ($P < 0.001$) between the sand ramp surfaces.

component loadings (ranging from 0.73 to 0.96), collectively explaining 54.1% of the total variance. These attributes included total soil organic carbon and its fractions (0.89–0.96), weathering indices (CIA, 0.86; CIW, 0.74; R, −0.94), mean weight diameter (MWD, 0.74), particle size distribution (−0.89 to 0.85), and oxides, specifically Fe_2O_3 (0.73), Al_2O_3 (0.85), K_2O (−0.91), CaO (−0.92), and Na_2O (−0.93). A significant correlation ($P < 0.01$) was observed among all these highly loaded attributes within PC1 (Fig. 8a). As indicated in Fig. 8b, the SOC 53–250 μm fraction, total SOC, MWD, CIW, RS, and fungal populations exhibited the highest weights.

We observed significant differences in the Soil Quality Index (SQI) between climbing and falling sand ramps (Fig. 8c). The climbing sand ramps exhibited a higher SQI value (0.73) compared to the falling surfaces (0.39). As shown in Fig. 8d, the contribution of SOC and the 53–250 μm fraction to the SQI was considerably higher on climbing sand ramps (30%) than on falling surfaces (1.70%). Furthermore, CIW, RS, PD, SiO_2, and BD contributed 26%, 24%, 20%, 19%, and 17% to the SQI, respectively. The results for falling sand ramps indicated a minimal contribution from variables affecting soil quality, specifically MWD, VWC, and bacterial populations (5–7%).

4. Discussion

4.1. Environmental dynamics across falling and climbing sand ramps

We examined the relationships between the evolution of sand ramp surfaces, environmental dynamics, associated geomorphic processes, and geochemical variations to evaluate the biogeochemical processes affecting the sequestration and mineralization of SOC within falling and climbing surfaces.

Based on the comparative analysis of granulometry, mineralogy, and grain morphology between climbing and falling sand ramps, the evidence supports the contribution of fluvial/alluvial processes (likely sheet wash or interaction with playa hydrology) in the formation of

Table 4
SOC correlation with sediment geochemistry within falling and climbing sand ramps.

Dependent variables	Explanatory variables	Standardized coefficient	Sig
Climbing sand ramp	SOC 53-250 μm	0.790	0.000
	MWD	0.450	0.000
	CIA	0.220	0.001
	GMD	0.016	0.019
	Fe_2O_3	0.014	0.022
	R	0.011	0.023
	Bacterial	0.009	0.031
Falling sand ramps	SOC > 250	0.63	0.000
	CCE	−0.37	0.005
	pH	−0.15	0.040

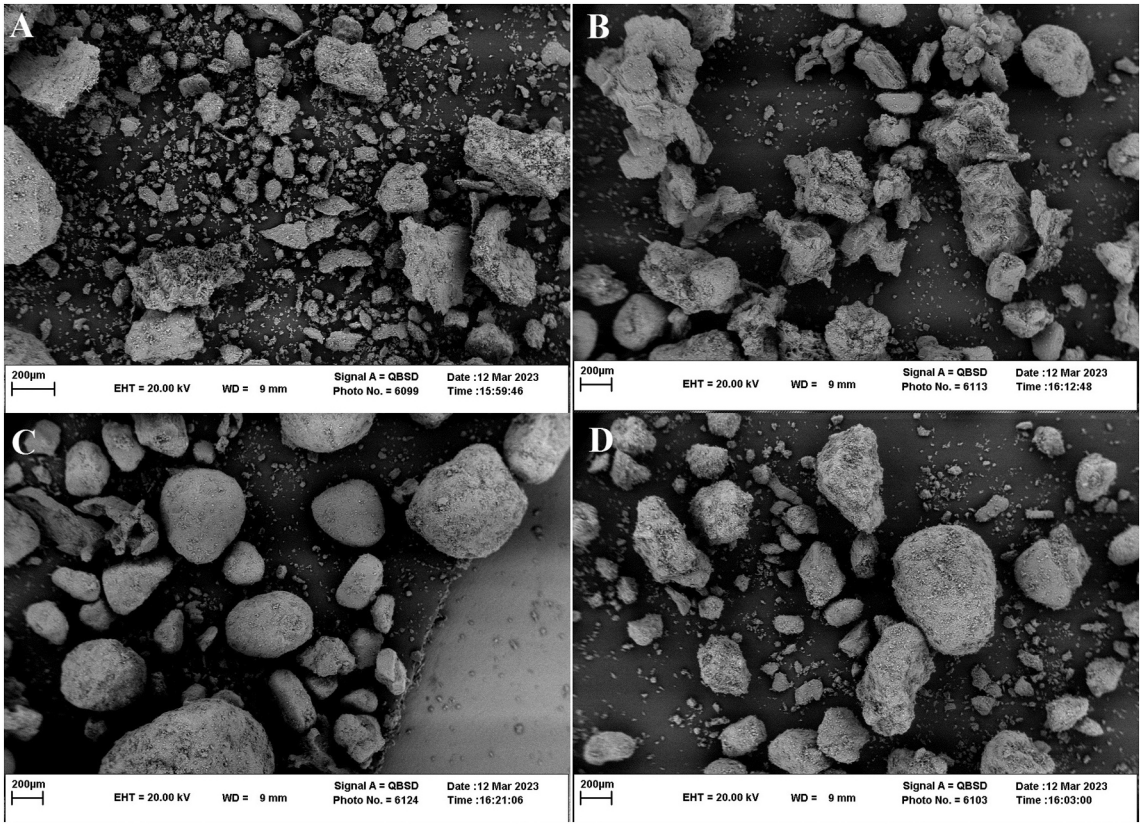

Fig. 6. Morphoscopy of climbing (A-B) and falling (C—D) sand ramps using scanning electron microscope (SEM) with a magnification of 60 and 120 times.

Table 5
Relationship between C mineralization ratio and sediment geochemistry within falling and climbing sand ramps.

Climbing sand ramp					
Variable	Unstandardized Beta	Standard Error	Standardized Beta	*P*-value	R-squared
Const	0.42	0.05		0.001	0.83
MWD	−0.09	0.02	−0.28	0.015	0.80
Fe_2O_3	−0.08	0.02	−0.25	0.010	0.80
GMD	−0.07	0.03	−0.24	0.025	0.74
SOC, 53–250	−0.11	0.04	−0.33	0.012	0.70
CIW	−0.08	0.03	−0.27	0.019	0.65

Falling sand ramp					
Variable	Unstandardized Beta	Standard Error	Standardized Beta	P-value	R-squared
const	0.31	0.04		0.0015	0.77
Bacterial_Population	0.08	0.03	0.36	0.018	0.74
SOC > 250	0.11	0.03	0.41	0.021	0.76

climbing ramps, in contrast to the purely aeolian/gravity-driven falling ramps. Consistent with this study and findings by others (Mycielska-Dowgiałło and Woronko, 2004; Woronko and Pisarska-Jamroży, 2016; Chmielowska et al., 2021), aeolian sediments display more rounded and spherical grains compared to fluvial deposits. Morphoscopic analysis clearly differentiates the transport mechanisms. Grains from climbing ramps (hydro-aeolian) are characterized by lower circularity and roundness, coupled with higher angularity. While aeolian transport typically rounds grains rapidly (Attal and Lavé, 2009; Domokos et al., 2014; Joo et al., 2018), the angularity observed here suggests two possibilities: (1) shorter transport distances from the alluvial source; or (2) the protection of grains within a fine-grained (muddy) matrix deposited by water, which buffers them against grain-to-grain collisions. Conversely, falling ramps (aeolian/gravity) exhibit high circularity and smoothness. This confirms a history dominated by aeolian abrasion and selective sorting by gravity, where rounder grains roll more easily. This strictly physical weathering pattern aligns with a dry, wind-dominated environment devoid of significant fluvial cohesive forces.

The most compelling evidence for fluvial influence is found in the grain size distribution statistics (Table 3). The climbing sand ramps exhibit very platykurtic distributions. Such distributions typically indicate a bimodal or poorly sorted mixture of two distinct sediment populations, implying the mixing of aeolian sands with fine-grained alluvial/lacustrine materials (silt and clay). In contrast, the falling sand ramps are leptokurtic, characteristic of a single dominant mode of transport (aeolian saltation/gravity). Furthermore, the climbing ramps are fine (positively) skewed, containing a substantial concentration of silt and clay. While aeolian dynamics remove fines through deflation, the retention of high percentages of fines (~71%) strongly points to aqueous deposition (e.g., settling from suspension in standing water or sheet floods) or sediment trapping by surface moisture, rather than pure wind transport.

Mineralogical data (XRD and XRF) exhibit chemical evidence for the presence of water. The abundance of secondary clay minerals (illite, kaolinite, and montmorillonite) alongside Fe/Al oxides in climbing ramps results directly from hydrolysis and chemical weathering, processes necessitating the prolonged presence of water. Consistent with this, the climbing ramps display higher CIA and CIW values, confirming a history of intense chemical alteration mediated by aqueous processes. Additionally, the presence of evaporites such as halite and anhydrite indicates a provenance associated with evaporitic environments (playas). Their incorporation into the climbing ramps suggests a genetic link to the fluctuating water tables and fluvial runoff of adjacent playas, where water transports both salts and fine-grained sediments.

Conversely, falling ramps range from near-symmetrical to negatively skewed and are sand-dominated, reflecting the winnowing action of aeolian processes. Granulometric, mineralogical (increasing unweathered minerals of quartz, orthoclase, dolomite, calcite, halite, and albite; Table 2 & Fig. 5a-c), and morphoscopic analyses (high circularity and solidity) suggest that falling sand ramps formed under recent arid conditions, mainly through aeolian processes and physical weathering. Further field observations found no evidence of colluvial/alluvial deposits or significant soil development, likely due to the short formation period and stable climate (Fig. 4A & C). Quartz, a highly weathering-resistant mineral, was dominant in falling sand ramps (>50%). The high frequency of carbonate minerals (Table 2 & Fig. 5a-c), sand sediments, well-sorted clastic aggregates, symmetrical grain distribution, high roundness, and minimal quartz corrosion suggest that these surfaces remain relatively intact, with limited evidence of weathering processes (see weathering indices in Table 1 & Fig. 6C-D). These characteristics indicate that the sediments had limited exposure to weathering processes. The XRD pattern of falling sand ramps showed stronger peaks for calcite, dolomite, and halite. Consequently, the limited exposure of falling sand ramps to weathering processes under the present warm climate could encourage the predominance of carbonate minerals.

Based on the findings, although macroscopic sedimentary structures were not the primary focus of this study, post-depositional processes and pedogenesis could obscure these features. However, this study demonstrated that the hydrologic signature in the climbing sand ramps is preserved at the microscopic and textural scales. While macroscopic bedding may be absent or obscured, the quantitative data conclusively demonstrate a divergence in formation processes. The falling sand ramps represent a classic, dry, unstable aeolian/gravitational system (coarse, sorted, rounded, and unweathered). The climbing sand ramps, however, represent a stabilized, hydro-aeolian system where wind transport interacts significantly with water availability (high fines, mixing of sediment grains, and chemical weathering products). Therefore, the differing environments of climbing and falling sand ramps, in terms of geomorphic and weathering processes and mineralogical dynamics, could affect the bio-geochemical mechanisms controlling the sequestration and mineralization of SOC across the evolution of sand ramps.

4.2. Role of environmental dynamics in mechanisms controlling SOC within sand ramps

Environmental variables controlling the temporal and spatial patterns of soil organic carbon have been explored in previous research (Chappell et al., 2019; Mohseni et al., 2023; Zhang et al., 2024; Kumar et al., 2024; Freitas et al., 2024; Qu et al., 2025; Chen et al., 2025; Leite et al., 2025). However, there remains a notable gap in understanding how environmental dynamics (see Sect. 4.1 for details) affect the biogeochemical processes regulating carbon sequestration and mineralization within falling and climbing sand ramps.

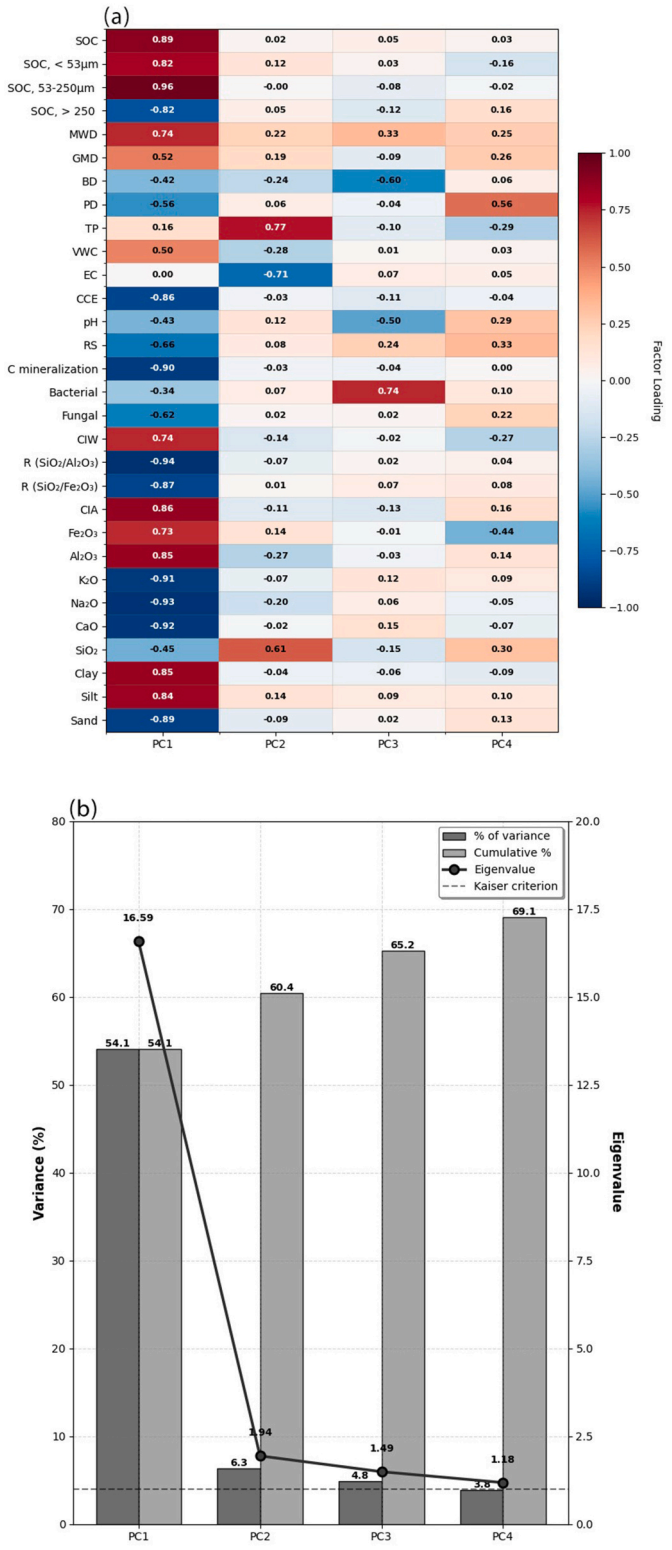

Fig. 7. (A) Results of principal component analysis showing soil quality indicators for the first four PCs; (B) Eigenvalue and variance percentage for the first four PCs.

As indicated in Table 4, the SOC fraction (53–250 µm), stability indices, weathering intensity, Fe_2O_3 content, and bacterial abundance exerted a significant positive influence on total SOC within climbing ramps. Based on XRF results and weathering indices (Table 1), climbing sand ramps exhibited a marked increase in weathering intensity, evidenced by higher CIA and CIW values, a lower R value, and elevated Al_2O_3 and Fe_2O_3 contents. Elucidating the relationships between soil stability indicators, weathering intensity, SOC fractions, and mineralogical composition helps explain the localized variations in factors controlling the C mineralization ratio across different sand ramp surfaces (Table 5). Despite possessing a higher total SOC content, climbing sand ramps exhibited a lower C mineralization rate. This pattern suggests the stabilization of organic carbon via chemical interactions with clay minerals, such as sorption, adsorption, and the formation of organo–mineral complexes on mineral surfaces (Wattel-Koekkoek et al., 2001; von Lützow et al., 2007). Such interactions limit microbial access to organic substrates, notwithstanding the elevated SOC levels. As evidenced by the XRD patterns (Table 2 & Fig. 5d-f), the abundance of secondary clay minerals (illite, kaolinite, and montmorillonite) alongside Fe_2O_3 and Al_2O_3 oxides in climbing sand ramps likely results from the prolonged chemical weathering and alteration of granitoid rocks. Furthermore, the prevalence of secondary minerals has promoted pedogenic processes, enhancing soil quality and microaggregate-associated carbon compared to falling ramps. Advanced weathering of primary minerals has facilitated soil structure development, thereby sequestering SOC within micro-aggregates for extended periods and rendering it less accessible to microbial mineralization. These findings accord with studies by Denef and Six (2005), Zech et al. (2020), Reichenbach et al. (2021), and Kirsten et al. (2021), which underscore the pivotal role of prolonged clay mineral weathering in carbon stabilization through organo-mineral associations.

Although sodium is commonly associated with clay dispersion and aggregate breakdown in agricultural soils, its role in sediment stability is highly context-dependent. In arid environments, $Na^+$and halite may increase mechanical stability by promoting salt cementation, pore-space filling, and surface crust formation, leading to higher compressive strength under dry conditions. This form of stability differs fundamentally from aggregate stability in moist soils, where sodium typically exerts a dispersive effect (Motaghi et al., 2020). Consequently, the stabilizing influence of Na^+observed in climbing sand ramps reflects short-term physicochemical strengthening rather than long-term pedogenic aggregation. Although carbonate minerals generally enhance soil bonding (Hamzehpour and Marcolli, 2024), their concentration in falling sand ramps may have an opposite effect. Despite the development of carbonate minerals on these surfaces, a lower percentage of clay particles and secondary minerals, combined with the dominance of quartz particles in the sand-sized fraction, weakens the soil bonding process, promoting reduced stability compared to climbing sand ramps. These conditions encourage a high susceptibility of these surfaces to C mineralization processes.

These findings explain why climbing sand ramps provide a more stable environment for SOC retention, where prolonged weathering, mineral formation, and organic matter interactions with mineral surfaces enhance SOC stability. The dominance of clay minerals in climbing sand ramps likely contributed to improved soil structure, as indicated by higher MWD and GMD values (Table 1). Additionally, increased porosity in these surfaces, associated with allophanic components (XRF results, Table 1), has been linked to greater protection of soil organic matter against microbial decomposition (Cuypers et al., 2002; Singh et al., 2017; Yang et al., 2017; Reichenbach et al., 2021). This is evident in the higher C sequestration observed in climbing surfaces, where greater porosity and microaggregate formation coincide with elevated sesquioxide content (such as ferrihydrite).

The interaction of sediment-laden aeolian flows with topographic obstacles induces a deceleration in flow velocity, stimulating substantial deposition of transported material. This mechanism is responsible for the poor sorting of sediments on climbing sand ramps, which characteristically contain a considerable fraction of fine-grained particles (e.g., silt and clay minerals) and evaporite minerals. This condition stimulates mineralogical heterogeneity within climbing surfaces, marked by the formation of minerals such as illite, montmorillonite, and anhydrite.

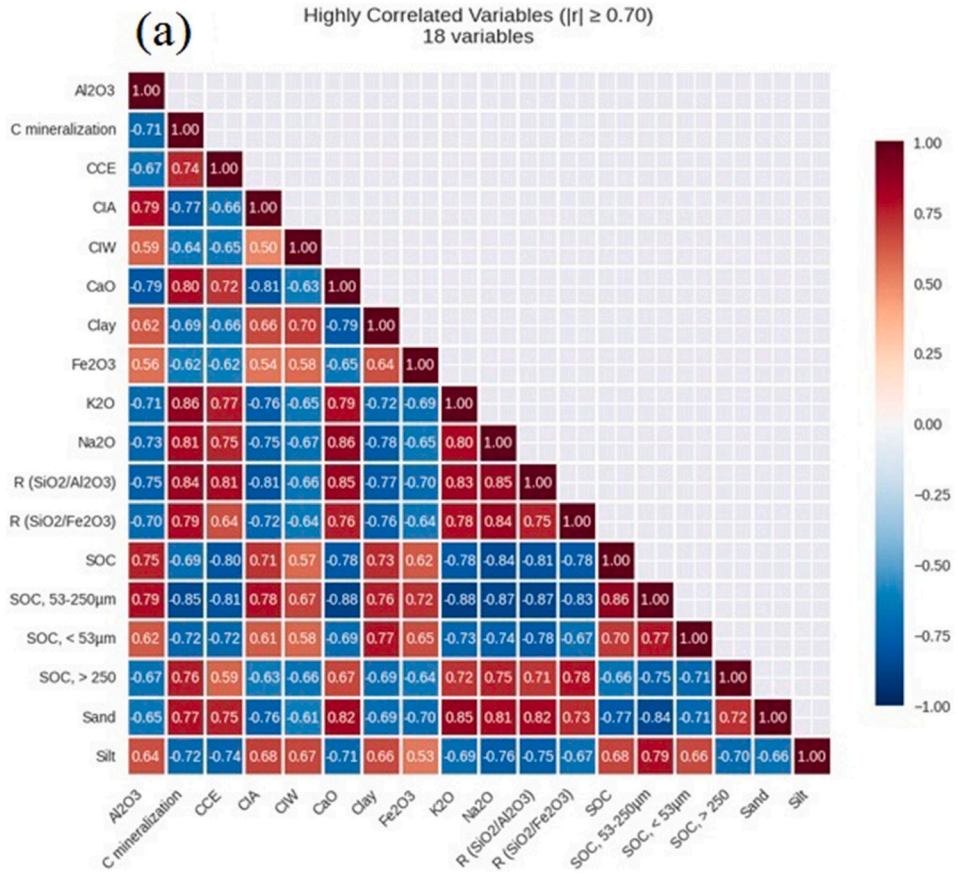

Fig. 8. (a) Correlation matrix of the highly-weighted variables; (b) The importance of MDS variables; (c) Soil quality index of the sand ramps; (d) Contribution of scored and weighted variables to the soil quality index of the studied sand ramps.

Consequently, the presence of clay minerals promotes aggregate formation and the subsequent stabilization of organic carbon. In contrast, as demonstrated by Lancaster and Tchakerian (1996) and Rowell et al. (2018b), falling sand ramps are generally situated at higher elevations and steeper gradients, where grainfall and grainflow processes predominate. This environment fosters a highly efficient winnowing effect, leading to particle segregation based on specific gravity and size, which results in better sorting compared to climbing surfaces. Consequently, denser particles (such as quartz and calcite) settle out on the inclined surface. Meanwhile, very fine particles, particularly clay minerals and organic matter, are kept in suspension by turbulent flow and are subsequently deposited at more distant locations. These characteristics systematically impede pedogenic processes and promote mineralogical homogeneity, dominated mainly by quartz and calcite, within falling surfaces. A decreased abundance of clay and evaporite minerals hinders soil development and long-term SOC stabilization within these ramps compared to climbing ones.

Comprehensive laboratory analyses and field observations confirm that particles within climbing sand ramps are aggregated through pedogenic processes, whereas falling sand ramps typically exhibit a dispersed, single-grain structure characteristic of aeolian transport. Although well-developed diagnostic soil horizons were not consistently observed—particularly on falling sand ramps—climbing surfaces occasionally displayed weak, incipient pedogenic development. The poor expression of soil horizons aligns with the *geomorphologically* active nature of these landforms and the prevailing arid to semi-arid conditions, where pedogenesis proceeds slowly, and horizon differentiation is limited. Consequently, soil development in this study was inferred primarily from mineralogical, geochemical, and structural proxies rather than classical profile morphology.

Under present-day environmental conditions, the results demonstrate distinct pedogenic pathways characterizing climbing and falling sand ramps. Climbing sand ramps exhibit active pedogenesis, defined by enhanced chemical weathering, authigenic clay mineral formation, and progressive structural organization. Elevated CIA and CIW values, higher Fe_2O_3 and Al_2O_3 concentrations, increased aggregate stability indices (MWD and GMD), and the dominance of microaggregate-associated SOC collectively indicate ongoing pedogenesis and effective stabilization of organic carbon via organo–mineral interactions. These processes reflect a relatively mature soil system where prolonged weathering and mineral transformations enhance SOC retention and suppress carbon mineralization rates.

The findings suggest that the climbing sand ramps are not simple active dunes but act as cumulative paleosol sequences. The granulometric analysis reveals that climbing surfaces are poorly sorted, fine-grained and positively fine-skewed. This statistical signature-specifically the high silt and clay content-is characteristic of pedogenic modification rather than pure aeolian sorting (which is observed in the well-sorted, symmetrical falling ramps). Further, the presence of microaggregate-associated carbon and high SOC indicates active or relic soil formation. The sedimentary structure in climbing ramps is effectively massive or weakly stratified because pedogenesis and bioturbation have homogenized the primary aeolian bedding. Therefore, the lack of distinct physical sedimentary structures (like cross-stratification) is, in itself, a significant finding supported by the high clay content and secondary minerals, marking these units as stabilized, soil-forming geomorphic surfaces rather than active transport corridors.

Conversely, falling sand ramps display limited pedogenic progress

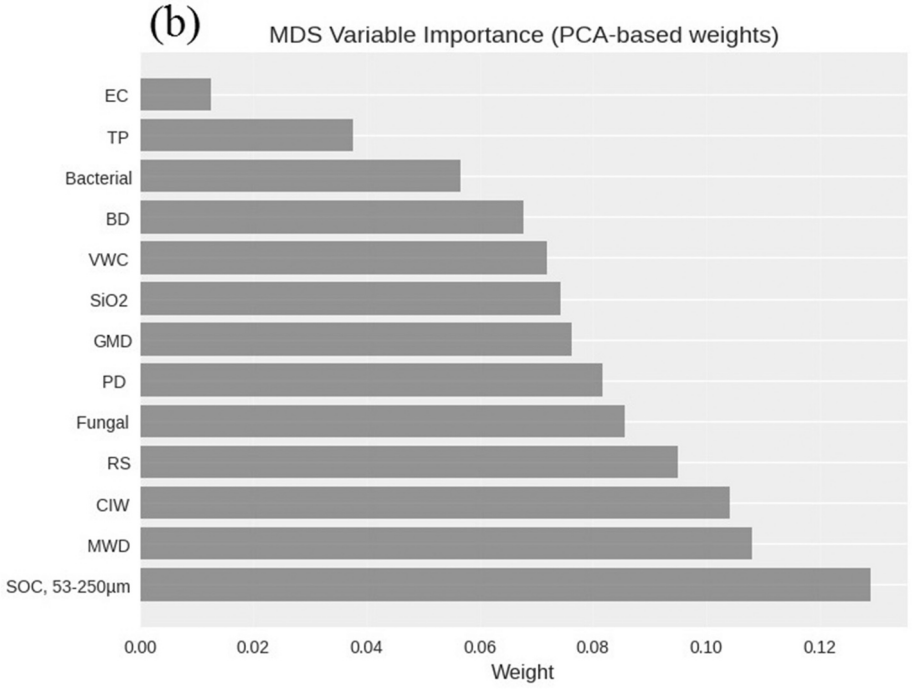

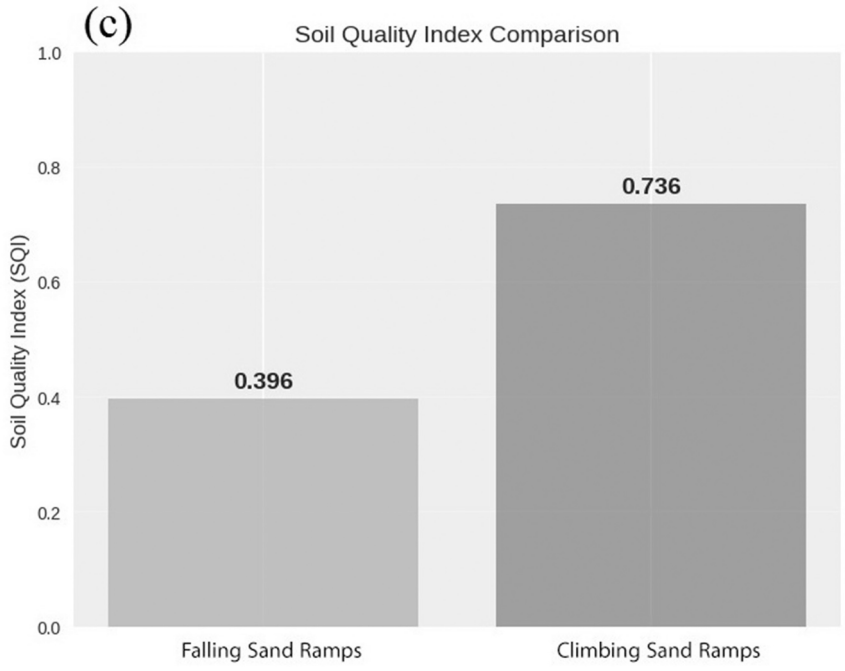

Fig. 8. (*continued*).

and are controlled predominantly by physical depositional and aeolian dynamics. These surfaces are influenced by dispersive salts (e.g., halite) and a scarcity of cementing clays, resulting in a mechanically dispersed state. The predominance of quartzose sand fractions, lower weathering indices, weak aggregate formation, and the prevalence of unprotected SOC fractions—coupled with higher soil respiration and carbon mineralization ratios—indicate minimal soil development. While sand ramps play a critical role in enhancing the geo-biodiversity of arid terrestrial ecosystems, their influence on SOC dynamics remains largely unexplored. Elucidating these processes is essential for assessing carbon storage potential and long-term ecological stability within these landscapes.

5. Conclusions

The quantitative data confirm that the textural differences (granulometry results) are physically linked to the morphological modifications (SEM results) observed in the sediments. The distinction between the angular, fine-grained climbing ramps and the rounded, coarse-grained falling ramps reflects a segregation of transport energy and duration. While climbing ramps typically represent angular saltating grains, the falling grains show signs of higher abrasion or selective sorting of rounder grains that roll more easily downslope (gravity-driven transport), consistent with the higher sorting values observed. The low circularity and solidity of the climbing grains suggest that transport

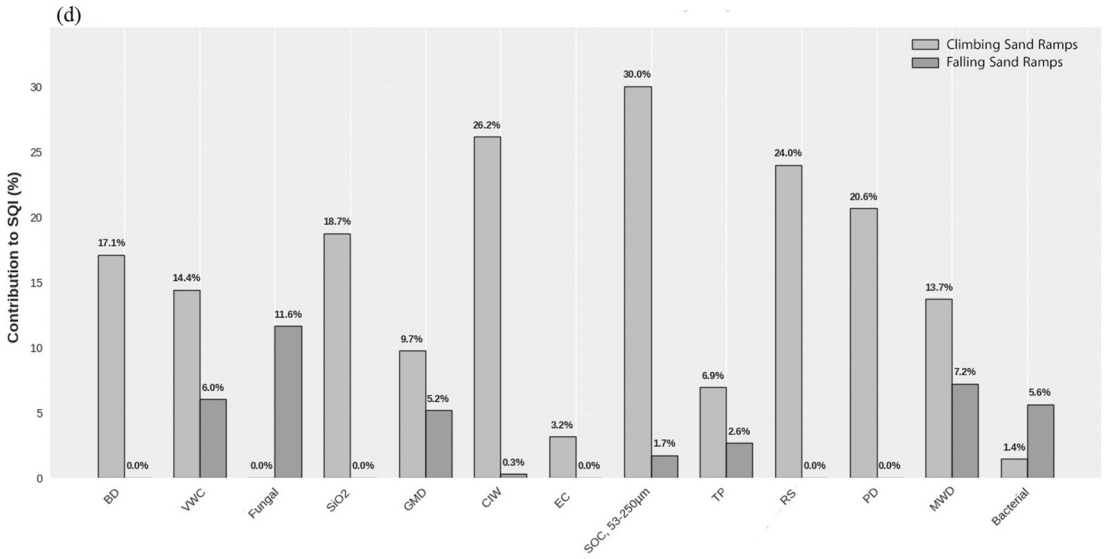

Fig. 8. (*continued*).

energy was sufficient to fracture grain edges, yet the transport distance was insufficient to smooth them. This statistical relationship confirms that morphological differences are not merely qualitative but represent measurable responses to transport distance and energy.

Granulometric, mineralogical, and morphoscopic analyses suggest that falling sand ramps formed under present climate conditions, influenced by aeolian processes and physical weathering. The prevalence of unweathered quartz minerals, carbonate minerals, sand sediments, and clastic aggregates, alongside high roundness, low angularity, high sorting, and low quartz corrosion, indicates that these environments remain relatively intact and less exposed to weathering. These characteristics have led to a greater abundance of coarse-sized SOC fractions, higher base cation concentrations, and elevated pH, which promoted incomplete microbial decomposition. Despite the development of carbonate minerals on the falling sand ramps, a lower percentage of clay particles and secondary minerals, combined with the dominance of quartz particles in the sand-sized fraction, weakens soil bonding processes, thereby reducing their stability compared to climbing sand ramps.

While sand-sized fractions, dominated by quartz particles, exhibit weak organic matter binding, clay phyllosilicate minerals effectively adsorb organic carbon through their multiple reactive pathways within climbing surfaces. Low roundness, low sorting, high angularity, and a high frequency of secondary clay minerals (illite, kaolinite, and montmorillonite), along with Fe_2O_3 and Al_2O_3 oxides, suggest long-term exposure of climbing surfaces to chemical weathering. These characteristics indicate that multiple processes—including physiochemical weathering, hydrological systems, and aeolian transport—contributed to the formation of climbing surfaces. Additionally, the greater presence of secondary minerals supported pedogenic processes, leading to improved soil quality and increased microaggregate-associated carbon compared to falling ramps. The findings demonstrate that climbing sand ramps represent a stabilized, pedogenically altered colluvial-aeolian apron overlying the granite, where primary sedimentary structures have been obscured by chemical weathering and clay illuviation, contrasting with the structurally intact, gravity-dominated falling ramps. Numerical dating of these sand ramps would further clarify how environmental dynamics of the Late Quaternary period and associated variations in mineralogical structures have influenced carbon turnover throughout the evolution of these landforms.

CRediT authorship contribution statement

Mohsen Kargarian: Resources, Investigation, Formal analysis, Data curation. **Neda Mohseni:** Writing – review & editing, Writing – original draft, Visualization, Supervision, Software, Methodology, Investigation, Funding acquisition, Formal analysis, Conceptualization. **Reza Hosseinzadeh:** Investigation.

Declaration of competing interest

The authors declare that they have no known competing financial interests or personal relationships that could have appeared to influence the work reported in this paper.

Acknowledgments

We would like to thank the two anonymous reviewers for their constructive and thoughtful comments, which significantly improved the quality of this manuscript. We are also grateful to the editor, Dr. Massimo Moretti, for his valuable guidance throughout the review process. This research was supported by Ferdowsi University of Mashhad, Mashhad, Iran (Grant No. 3-57534), whose financial and institutional assistance made this work possible.

Data availability

Data will be made available on request.

References

Andrews, S.S., Karlen, D.L., Mitchell, J.P., 2002. A comparison of soil quality indexing methods for vegetable production systems in Northern California. Agriculture, Ecosystems and Environment 90, 25–45.

Armenise, E., Redmile-Gordon, M.A., Stellacci, A.M., Ciccarese, A., Rubino, P., 2013. Developing a soil quality index to compare soil fitness for agricultural use under different managements in the Mediterranean environment. Soil and Tillage Research 130, 91–98.

Attal, M., Lavé, J., 2009. Pebble abrasion during fluvial transport: Experimental results and implications for the evolution of the sediment load along rivers. Journal of Geophysical Research: Earth Surface 114 (F4).

Bateman, M.D., Bryant, R.G., Foster, I.D., Livingstone, I., Parsons, A.J., 2012. On the formation of sand ramps: a case study from the Mojave Desert. Geomorphology 161, 93–109.

Bavel, C.V., 1949. Mean weight-diameter of soil aggregates as a statistical index of aggregation. Soil Science Society of America Journal 14, 20–23.

Beylich, A., Oberholzer, H.R., Schrader, S., Höper, H., Wilke, B.M., 2010. Evaluation of soil compaction effects on soil biota and soil biological processes in soils. Soil and Tillage Research 109, 133–143.
Blake, G.R., Hartge, K.H., 1986. Particle density. Methods of soil analysis: Part 1 physical and mineralogical methods 5, 377–382.
Chappell, A., Baldock, J.A., 2016. Wind erosion reduces soil organic carbon sequestration falsely indicating ineffective management practices. Aeolian Research 22, 107–116.
Chappell, A., Webb, N.P., Leys, J.F., Waters, C.M., Orgill, S., Eyres, M.J., 2019. Minimising soil organic carbon erosion by wind is critical for land degradation neutrality. Environmental Science & Policy 93, 43–52.
Chen, Y., Xi, H., Cheng, W., 2025. Spatiotemporal dynamics of soil organic carbon in desert region and its response to climate change: a case study of Heihe river. Ecological Indicators 170, 113005.
Chmielowska, D., Woronko, B., Dorocki, S., 2021. Applicability of automatic image analysis in quartz-grain shape discrimination for sedimentary setting reconstruction. Catena 207, 105602.
Chojnacki, M., Moersch, J.E., Burr, D.M., 2010. Climbing and falling dunes in Valles Marineris. Mars. Geophysical Research Letters 37, L08202.
Cuypers, C., Grotenhuis, T., Nierop, K.G.J., Franco, E.M., de Jager, A., Rulkens, W., 2002. Amorphous and condensed organic matter domains: the effect of per-sulfate oxidation on the composition of soil/sediment organic matter. Chemosphere 48, 919–931.
Damiba, W.A.F., Gathenya, J.M., Raude, J.M., Home, P.G., 2024. Soil quality index (SQI) for evaluating the sustainability status of Kakia-Esamburmbur catchment under three different land use types in Narok County. Kenya. Heliyon 10, e25611.
del Valle, L., Gómez-Pujol, L., Fornós, J.J., Timar-Gabor, A., Anechitei–Deacu, V., Pomar, F., 2016. Middle to late Pleistocene dunefields in rocky coast settings at Cala Xuclar (Eivissa, Western Mediterranean): Recognition, architecture and luminescence chronology. Quaternary International 407, 4–13.
Denef, K., Six, J., 2005. Clay mineralogy determines the importance of biological versus abiotic processes for macroaggregate formation and stabilization. European Journal of Soil Science 56, 469–479.
Deng, Y., Yu, L., Huang, Y., Zhang, S., 2023. Numerical Evaluation on Effects of Upstream Sand-Dune-shaped Ramp and Backward Coolant Injection on Heat transfer. Journal of Physics: Conference Series 2441, 012014.
Doetterl, S., Berhe, A.A., Nadeu, E., Wang, Z., Sommer, M., Fiener, P., 2016. Erosion, deposition and soil carbon: a review of process-level controls, experimental tools and models to address C cycling in dynamic landscapes. Earth-Science Reviews 154, 102–122.
Domokos, G., Jerolmack, D.J., Sipos, A.Á., Török, Á., 2014. How river rocks round: resolving the shape-size paradox. PLoS One 9, e88657.
Ellwein, A.L., Mahan, S.A., McFadden, L.D., 2015. Impacts of climate change on the formation and stability of late Quaternary sand sheets and falling dunes, Black Mesa region, southern Colorado Plateau, USA. Quaternary International 362, 87–107.
Folk, R.L., Ward, W.C., 1957. Brazos River bar [Texas]; a study in the significance of grain size parameters. Journal of Sedimentary Research 27, 3–26.
Freitas, V.S., Babos, D.V., Guedes, W.N., Silva, F.P., de Lima Tozo, M.L., Andrade, C.A., Martin-Neto, L., 2024. Soil organic matter dynamics and soil carbon stocks from tropical and sub-tropical areas under no-till: an on-farm research. Catena 247, 108491.
Gresina, F., Farkas, B., Fábián, S.Á., Szalai, Z., Varga, G., 2023. Morphological analysis of mineral grains from different sedimentary environments using automated static image analysis. Sedimentary Geology 455, 106479.
Hamzehpour, N., Marcolli, C., 2024. Soil crust development on playa surfaces of Lake Urmia and its controlling factors: New insights to combat dust sources. Catena 237, 107799.
Harnois, L., 1988. The CIW index: a new chemical index of weathering. Sedimentary Geology 55, 319–322.
Hay, A.S., Powell, D.M., Carr, A.S., Livingstone, I., 2021. Characterisation of aeolian sediment accumulation and preservation across complex topography. Geomorphology 383, 107704.
Jiang, Y., Gao, Y., He, C., Liu, B., Pan, Y., Li, X., 2021. Spatiotemporal distribution and variation of wind erosion over the Tibetan Plateau based on a coupled land-surface wind-erosion model. Aeolian Research 50, 100699.
Jin, J.H., Li, Z.Z., Cheng, Y., Xu, X.L., Li, Z.X., Liu, X.J., 2018. Late Pleistocene aeolian activity in Haitan Island, Southeast China: Insights from optically stimulated luminescence dating of coastal dunes on marine terraces. Journal of Mountain Science 15, 1777–1788.
Joo, Y.J., Soreghan, A.M., Madden, M.E.E., Soreghan, G.S., 2018. Quantification of particle shape by an automated image analysis system: a case study in natural sediment samples from extreme climates. Geosciences Journal 22, 525–532.
Kemper, W.D., Rosenau, R.C., 1986. Aggregate stability and size distribution. Methods of soil analysis: part 1. Physical and Mineralogical Methods 5, 425–442.
Kirsten, M., Mikutta, R., Kimaro, D.N., Feger, K.H., Kalbitz, K., 2021. Aluminous clay and pedogenic Fe oxides modulate aggregation and related carbon contents in soils of the humid tropics. Soil 7, 363–375.
Kumar, A., Srivastava, P., Meena, N.K., 2017. Late Pleistocene aeolian activity in the cold desert of Ladakh: a record from sand ramps. Quaternary International 443, 13–28.
Kumar, J., Bhardwaj, D.R., Thakur, C.L., Sharma, P., Sharma, P., 2024. Soil organic carbon dynamics under different land use systems in dry temperate ecosystem of North-Western Himalayas. Catena 240, 108022.
Lal, R., 2019. Accelerated soil erosion as a source of atmospheric CO2. Soil and Tillage Research 188, 35–40.
Lancaster, N., Tchakerian, V.P., 1996. Geomorphology and sediments of sand ramps in the Mojave Desert. Geomorphology 17, 151–165.
Leite, F.F.G.D., Fontana, A., Nóbrega, G.N., Santos, F.M., Alves, B.J.R., da Silveira, J.G., Rodrigues, R.D.A.R., 2025. Land use change effect on organic matter dynamics and soil carbon sequestration in the Brazilian Cerrado: a study case in Mato Grosso do Sul state (Midwest-Brazil). Catena 249, 108670.
Li, Y., Zhao, H., Liu, J., Chaonan, C., Yuxuan, G., 2024. A framework for selecting and assessing soil quality indicators for sustainable soil management in waste dumps. Scientific Reports 14, 8491.
Loeppert, R.H., Suarez, D.L., 1996. Carbonate and gypsum. In: Sparks, D.L. (Ed.), Methods of Soil Analysis. Part 3. Chemical Methods. Soil Science Society America, Madison, pp. 437–474.
Martewicz, J., Kalińska, E., Weckwerth, P., 2022. What hides in the beach sand? A multiproxy approach and new textural code to recognition of beach evolution on the southern and eastern Baltic Sea coast. Sedimentary Geology 435, 106154.
Mazurak, A.P., 1950. Effect of gaseous phase on water-stable synthetic aggregates. Soil Science 69, 135–148.
Mohseni, A., Mohseni, N., Karimi, A., Egli, M., 2023. Interactions of soil quality, ages of alluvial fans, and mechanisms controlling total soil organic carbon dynamics. Catena 232, 107413.
Motaghi, F.A., Hamzehpour, N., Abasiyan, S.M.A., Rahmati, M., 2020. The wind erodibility in the newly emerged surfaces of Urmia Playa Lake and adjacent agricultural lands and its determining factors. Catena 194, 104675.
Mycielska-Dowgiałło, E., Woronko, B., 2004. The degree of aeolization of Quaternary deposits in Poland as a tool for stratigraphic interpretation. Sedimentary Geology 168, 149–163.
Nesbitt, H., Young, G.M., 1982. Early Proterozoic climates and plate motions inferred from major element chemistry of lutites. Nature 299, 715–717.
Osman, M.B., Tierney, J.E., Zhu, J., Tardif, R., Hakim, G.J., King, J., Poulsen, C.J., 2021. Globally resolved surface temperatures since the last Glacial Maximum. Nature 599, 239–244.
Pinet, S., Lartiges, B., Martinez, J.M., Ouillon, S., 2019. A SEM-based method to determine the mineralogical composition and the particle size distribution of suspended sediment. International Journal of Sediment Research 34, 85–94.
Qu, Q., Xu, H., Xu, L., You, C., Tan, B., Li, H., Wang, M., 2025. Forest thinning effects on soil carbon stocks and dynamics: Perspective of soil organic carbon sequestration rates. Catena 250, 108759.
Rabbi, S.F., Wilson, B.R., Lockwood, P.V., Daniel, H., Young, I.M., 2014. Soil organic carbon mineralization rates in aggregates under contrasting land uses. Geoderma 216, 10–18.
Reichenbach, M., Fiener, P., Garland, G., Griepentrog, M., Six, J., Doetterl, S., 2021. The role of geochemistry in organic carbon stabilization against microbial decomposition in tropical rainforest soils. Soil 7, 453–475.
Richards, L.A., 1954. Diagnosis and Improvement of Saline and Alkali Soils. U.S. Dept. of. Agriculture 78, 154.
Rowell, A., Thomas, D., Bailey, R., Stone, A., Garzanti, E., Padoan, M., 2018b. Controls on sand ramp formation in southern Namibia. Earth Surface Processes and Landforms 43, 150–171.
Rowell, A.L., Thomas, D.S., Bailey, R.M., Holmes, P.J., 2018a. Sand ramps as palaeoenvironmental archives: Integrating general principles and regional contexts through reanalysis of the Klipkraal Sands, South Africa. Geomorphology 311, 103–113.
Rowell, D.L., 1994. Soil Science: Methods & Applications. Longman Scientific & Technical, Harlow, UK.
Ruxton, B.P., 1968. Measures of the degree of chemical weathering of rocks. Journal of Geology 76, 518–527.
Sheibi, M., Esmaelly, D., 2009. Geological and residual evidence of restoration in anataksi shirkouh granite, southeast of Yazd. Iranian Journal of Crystallography and Mineralogy 18, 135–146.
Singh, M., Sarkar, B., Biswas, B., Bolan, N.S., Churchman, G.J., 2017. Relationship between soil clay mineralogy and carbon protection capacity as influenced by temperature and moisture. Soil Biology and Biochemistry 109, 95–106.
Six, J., Feller, C., Denef, K., Ogle, S., de Moraes Sa, J.C., Albrect, A., 2002. Soil organic matter, biota and aggregation in temperate and tropical soils – effects of no tillage. Agronomie 22, 755–775.
Telfer, M.W., Thomas, Z.A., Breman, E., 2012. Sand ramps in the Golden Gate Highlands National Park, South Africa: evidence of periglacial aeolian activity during the last glacial. Palaeogeography, Palaeoclimatology, Palaeoecology 313, 59–69.
Tesfahunegn, G.B., 2014. Soil quality assessment strategies for evaluating soil degradation in Northern Ethiopia. Applied and Environmental Soil Science 1, 646502.
Van Hateren, J.A., Van Buuren, U., Arens, S.M., Van Balen, R.T., Prins, M.A., 2020. Identifying sediment transport mechanisms from grain size–shape distributions, applied to aeolian sediments. Earth Surface Dynamics 8, 527–553.
Varga, G., Dagsson-Waldhauserová, P., Gresina, F., Helgadottir, A., 2021. Saharan dust and giant quartz particle transport towards Iceland. Scientific Reports 11, 11891.
von Lützow, M., Kögel-Knabner, I., Ekschmitt, K., Flessa, H., Guggenberger, G., Matzner, E., Marschner, B., 2007. SOM fractionation methods: relevance to functional pools and to stabilization mechanisms. Soil Biology and Biochemistry 39, 2183–2207.
Wattel-Koekkoek, E.J.W., Van Genuchten, P.P.L., Buurman, P., Van Lagen, B., 2001. Amount and composition of clay-associated soil organic matter in a range of kaolinitic and smectitic soils. Geoderma 99, 27–49.
Webb, N.P., Van Zee, J.W., Karl, J.W., Herrick, J.E., Courtright, E.M., Billings, B.J., Van Pelt, R.S., 2017. Enhancing wind erosion monitoring and assessment for US rangelands. Rangelands 39, 85–96.
Wollum, A.G., 1982. Cultural methods for soil microorganisms. In: Methods of Soil Analysis: Part 2 Chemical and Microbiological Properties, 9, pp. 781–802.

Woronko, B., Pisarska-Jamroży, M., 2016. Micro-scale frost weathering of sand-sized quartz grains. Permafrost and Periglacial Processes 27, 109–122.
Yang, C., Che, Y., Qi, Y., Liang, P., Song, C., 2017. High throughput sequencing of viable microbial communities in raw pork subjected to a fast-cooling process. Journal of Food Science 82, 145–153.
Zech, S., Dultz, S., Guggenberger, G., Prechtel, A., Ray, N., 2020. Microaggregation of goethite and illite evaluated by mechanistic modeling. Applied Clay Science 198, 105845.
Zhang, C., Chen, Y., Wei, Y., Yu, P., Hong, Y., Hu, Y., Shi, Z., 2024. Unraveling the threshold and interaction effects of environmental variables on soil organic carbon mapping in plateau watershed. Geoderma 450, 117032.